Journal of Catalysis 259 (2008) 138–146

Contents lists available at ScienceDirect

Journal of Catalysis

www.elsevier.com/locate/jcat

Promoting effect of Co addition on the catalytic partial oxidation of methane at short contact time over a Rh/MgO catalyst

Seiji Naito [a], Hisanori Tanaka [a], Shigeru Kado [a,1], Toshihiro Miyao [b], Shuichi Naito [b], Kazu Okumura [c], Kimio Kunimori [a], Keiichi Tomishige [a,*]

[a] Institute of Materials Science, University of Tsukuba, 1-1-1 Tennodai, Tsukuba, Ibaraki 305-8573, Japan
[b] Department of Material and Life Chemistry, Kanagawa University, 3-27-1 Rokkakubashi, Kanagawa-ku, Yokohama 221-8686, Japan
[c] Department of Materials Science, Faculty of Engineering, Tottori University, Koyama-cho Minami, Tottori 680-8552, Japan

ARTICLE INFO

Article history:
Received 1 June 2008
Revised 2 August 2008
Accepted 5 August 2008
Available online 30 August 2008

Keywords:
Catalytic partial oxidation
Methane
Thermography
Hot spot
Rhodium
Cobalt
Alloy

ABSTRACT

In catalytic partial oxidation of methane under isothermal conditions, a 0.3 wt% Rh/MgO catalyst modified with Co at a molar ratio of Co/Rh = 1 gave greater CH_4 conversion and selectivity to CO and H_2 than unmodified 0.3 wt% Rh/MgO. Characterization results using temperature-programmed reduction, extended X-ray absorption fine structure, and transmission electron microscopy demonstrated alloy formation between Rh and Co. In catalytic partial oxidation of methane without N_2 dilution, the Rh–Co/MgO catalyst with Co/Rh = 1 suppressed the temperature increase near the catalyst bed inlet and yielded a flat temperature profile. This behavior can be interpreted as greater selectivity in the direct partial oxidation route in the presence of gas-phase oxygen and lower activity in the steam reforming of methane in the absence of gas-phase oxygen. The better performance of Rh–Co/MgO (Co/Rh = 1) compared with Rh/MgO may result from greater methane dissociation and reduction degree during the partial oxidation of methane.

© 2008 Elsevier Inc. All rights reserved.

1. Introduction

The production of synthesis gas from natural gas is important in gas-to-liquid processes and methanol synthesis [1,2]. Steam reforming of methane has been used conventionally in industry [2–5]. Conventional steam reformers are large and expensive because steam reforming of methane is a highly endothermic reaction, as shown in Eq. (1); the reactor must be heated from the outside. Recently, much attention has focused on catalytic partial oxidation of methane [Eq. (2)] as a compact method for synthesis gas production:

$$CH_4 + H_2O \rightarrow CO + 3H_2, \quad \Delta H^0_{298\,K} = +206\ \mathrm{kJ\,mol^{-1}}, \tag{1}$$

$$CH_4 + (1/2)O_2 \rightarrow CO + 2H_2, \quad \Delta H^0_{298\,K} = -36\ \mathrm{kJ\,mol^{-1}}. \tag{2}$$

High methane conversion and syngas yield have been obtained at short and millisecond contact times in the catalytic partial oxidation of methane [6–13]. Various supported metal catalysts have been tested, and Rh has been found to be an effective component [7,8]. However, the reports on bimetallic catalysts containing Rh are so limited [14]. The alloy formation of Pt, Pd, and Rh with Ni has been reported to be effective to the oxidative steam reforming of methane in terms of the catalytic activity and the suppression of hot spot formation [15,16]. This property is attributed to maintenance of the Ni metal species even in the presence of gas-phase oxygen through the alloy formation between Ni and noble metals. These previous studies suggest that the alloying between a noble metal and a base metal can be connected to synergetic effects, which allow the substitution of a noble metal with a base metal.

In the present study, the effect of adding Co, Ni, and Fe over Rh/MgO was investigated. An effective modification can decrease the use of Rh, which has high cost and limited availability. In particular, the effect of modifiers on the temperature profiles of the catalyst bed, as well as the methane conversion and selectivity for synthesis gas formation, also were investigated.

Hot spot formation is a common problem in the conversion of hydrocarbons to synthesis gas using oxygen in catalytic partial oxidation [17–20] and the oxidative reforming of methane [15,16,21,22]. This phenomenon is attributable to the combustion reaction [Eq. (3)] over catalysts near the bed inlet, which can cause catalyst deactivation through sintering of support materials and aggregation of active metal particles:

$$CH_4 + 2O_2 \rightarrow CO_2 + 2H_2O, \quad \Delta H^0_{298\,K} = -803\ \mathrm{kJ\,mol^{-1}}. \tag{3}$$

Here we report that the addition of Co to 0.3 wt% Rh/MgO in a suitable amount enhanced CH_4 conversion and selectivity for syn-

* Corresponding author. Fax: +81 29 853 5030.
E-mail address: tomi@tulip.sannet.ne.jp (K. Tomishige).
[1] Present address: Research & Development Center, CHIYODA Corporation, 3-13 Moriya-cho, Kanagawa-ku, Yokohama, Kanagawa 221-0022, Japan.

0021-9517/$ – see front matter © 2008 Elsevier Inc. All rights reserved.
doi:10.1016/j.jcat.2008.08.002

gas formation beyond that of 1.0 wt% Rh/MgO in the partial oxidation of methane at short contact time. Our findings also demonstrate that Rh/MgO modified with an optimum amount of Co was very effective in suppressing hot spot formation. This high performance resulted from alloy formation between Rh and Co based on the catalyst characterization.

2. Experimental

2.1. Catalyst preparation

Rh/MgO catalysts were prepared by impregnating MgO with an aqueous solution of $RhCl_3 \cdot 3H_2O$ (Soekawa Chemicals). The MgO was obtained by calcining $MgCO_3$ (Wako Pure Chemical Industries Ltd.) at 1423 K for 3 h; the BET surface area of the MgO was determined to be 6.5 $m^2\,g^{-1}$. After impregnation, the solvent was evaporated at 353 K, and the resulting sample was dried at 383 K for 12 h and then calcined at 773 K for 3 h. The loading amounts of Rh were 0.3–3.2 wt%. In addition, Rh/MgO modified with additive metals also was prepared. Co, Ni, and Fe were added by the co-impregnation method using a mixed aqueous solution of $RhCl_3 \cdot 3H_2O$ and corresponding nitrate. After co-impregnation, the solvent was evaporated at 353 K, and the resulting sample was dried at 383 K for 12 h, then calcined at 773 K for 3 h. $Co(NO_3)_2 \cdot 6H_2O$, $Ni(NO_3)_2 \cdot 6H_2O$, and $Fe(NO_3)_3 \cdot 9H_2O$ were obtained from Wako Pure Chemical Industries. The catalysts are designated Rh–M/MgO, and the amount of the additives is described by the molar ratio of Rh, as in Rh–Co/MgO (Co/Rh = 1). The loading amount of Rh on Rh–M/MgO (M = Co, Ni, Fe) was 0.3 wt%. As a reference, 0.2 wt% Co/MgO was prepared using the impregnation method. A loading amount of 0.2 wt% Co corresponded to a Co amount on Rh–Co/MgO (Co/Rh = 1). In addition, 0.6 wt% Rh–Co/MgO (Co/Rh = 1) also was prepared. Catalysts in powder form were pressed, then crushed and sieved into granules of 0.13–0.18 mm. After reduction at 1123 K for 0.5 h, the BET surface area of 0.3 wt% Rh/MgO was determined to be 5.6 $m^2\,g^{-1}$, and the BET surface areas of Rh–M/MgO (M = Co, Ni, and Fe, M/Rh = 1) were determined to be 5.1, 7.5, and 5.7 $m^2\,g^{-1}$, respectively.

2.2. Catalytic performance in the partial oxidation of methane under isothermal conditions

Activity tests for the partial oxidation of methane were carried out using a quartz tubular fixed-bed flow reactor. A thin quartz tube was inserted into the catalyst bed as a thermowell, as illustrated in Fig. 1a. A thermocouple at the bottom of the catalyst bed monitored and controlled the reaction temperature by furnace heating. The catalyst weight was 10 mg. The catalyst samples were reduced with hydrogen at 1123 K for 0.5 h before each activity test. To prevent a temperature increase of the catalyst bed due to exothermic reactions, the reactant gases ($CH_4 + O_2$) were well diluted with N_2 up to $CH_4/O_2/N_2 = 4/2/94$. No temperature increases were found by infrared thermography. The total gas flow rate was 1500 $cm^3\,min^{-1}$, and the contact time was as short as 0.4 ms. Catalytic performance was examined for 0.5 h; steady-state activity and selectivity are shown. The effluent gas was analyzed using an FID-GC equipped with a methanator for CO, CH_4, and CO_2 and a TCD-GC (with Ar as carrier gas) for H_2 and a TCD-GC (with He as carrier gas) for O_2. Methane conversion and CO and H_2 selectivity were calculated as follows:

$$\mathrm{CH_4\ conversion\ (\%)} = \frac{(C_{CO} + C_{CO_2})}{(C_{CH_4} + C_{CO} + C_{CO_2})} \times 100,$$

$$\mathrm{CO\ selectivity\ (\%)} = \frac{C_{CO}}{(C_{CO} + C_{CO_2})} \times 100,$$

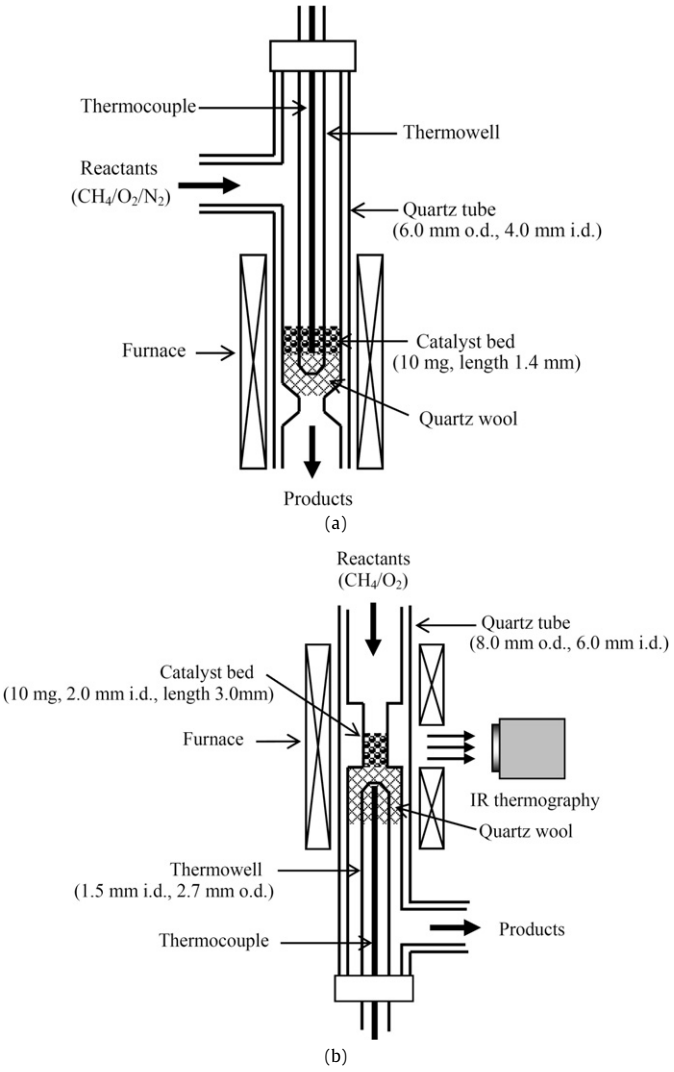

Fig. 1. Reactor setup: (a) partial oxidation of methane with N_2 dilution for isothermal conditions, (b) partial oxidation of methane without N_2 dilution for the IR thermographical observation.

and

$$\mathrm{H_2\ selectivity\ (\%)} = \frac{C_{H_2}}{((C_{CO} + C_{CO_2}) \times 2)} \times 100,$$

where C is the concentration of each component in the effluent gases. Throughout all of the experiments, no carbon-containing products other than CO and CO_2 were formed. The amount of carbonaceous materials, such as coke deposited on the catalyst surface, was negligible.

2.3. Temperature measurement of catalyst bed with infrared thermography

Reaction tests for partial oxidation of methane ($CH_4/O_2 = 2/1$) without N_2 dilution were carried out using a fixed-bed quartz reactor, as depicted in Fig. 1b, using IR thermography (TH31; NEC San-ei Instruments Ltd.). Because temperature profiles dependent strongly on catalytic property and performance under the reaction conditions, the profiles were measured using IR thermography, as reported previously [16,23]. The catalyst sample weighed 10 mg, and the bed was 3.0 mm long. The furnace temperature was controlled at 723 K. A cooling trap was located at a reactor exit to remove steam contained in effluent gases. Gas analysis was the same

as that used for the activity test in the partial oxidation of methane under isothermal conditions. In experiments for measuring the effect of steam addition to the partial oxidation of methane, steam was obtained by vaporizing distilled water supplied using a feeding pump.

2.4. Characterization of catalysts

Temperature-programmed reduction (TPR) profiles were measured in a fixed-bed quartz reactor. Before TPR measurement, catalysts were treated in O_2 at 773 K for 0.5 h and then in Ar at 773 K for 0.5 h, to remove adsorbed species such as CO_2. The sample weight was 50 mg. The heating rate was 10 K min^{-1} from room temperature to 1123 K, and 5% H_2 diluted in Ar (30 cm^3 min^{-1}) was used. A cold trap with frozen acetone (ca. 173 K) was used to remove any steam formed. TPR profiles were monitored continuously using an online TCD-GC. Hydrogen consumption was estimated from the integrated peak area of the profiles.

Measurement of H_2 chemisorption was carried out in a high-vacuum system using a volumetric method. Before adsorption of H_2, the catalyst sample was treated in H_2 at 1123 K for 0.5 h in a fixed-bed reactor. After this pretreatment, the sample was transferred to a cell for adsorption measurements under air atmosphere. Before each measurement, H_2 pretreatment was carried out at 773 K for 0.5 h in the cell. After evacuation at 773 K, the sample was cooled to room temperature. The total amount of H_2 adsorption was measured at room temperature, with a H_2 pressure at adsorption equilibrium of about 2.6 kPa. The dead volume of the apparatus was 63.5 cm^3, and the sample weight was 150 mg.

Transmission electron microscopy (TEM) images were obtained using a JEOL JEM-2010F microscope operating at 200 kV. Catalysts were reduced by H_2 pretreatment at 1123 K for 0.5 h or used for activity tests in the partial oxidation of methane without N_2 dilution for 3.0 h. Samples were dispersed in 2-propanol using supersonic waves, then placed on Cu grids for TEM observation under air atmosphere. On the TEM images, small and dark spheres can be assigned to metal particles containing Rh and/or Co. More than 100 particles were measured on several images; particle size ranged from 1 to 11 nm. Average particle size (d) was calculated by $d = \sum n_i d_i^3 / \sum n_i d_i^2$, where n_i is the number of pieces and d_i is the particle size [24].

Rh K-edge EXAFS were measured at BL01B1 station in SPring-8 with support from the Japan Synchrotron Radiation Research Institute (JASRI) (proposal 2006A1058). The storage ring was operated at 8 GeV. A Si (311) single crystal was used to obtain a monochromatic X-ray beam. Two ion chambers filled with 50% Ar + 50% N_2 and 75% Ar + 25% Kr were used to detect I_0 and I, respectively. Co K-edge EXAFS was measured at BL-9C station of the Photon Factory at the High-Energy Accelerator Research Organization (proposal 2006G095). The storage ring was operated at 2.5 GeV. A Si(111) single crystal was used to obtain a monochromatic X-ray beam. The monochromator at both rings was detuned to 60% maximum intensity, to avoid higher harmonics in the X-ray beam. Two ion chambers filled with N_2 and 25% Ar diluted with N_2 for Co K-edge EXAFS were used to detect I_0 and I, respectively. Samples for the EXAFS measurement were prepared by pressing catalyst powders of 750 mg for Rh and 250 mg for Co K-edge EXAFS. The catalyst powder was treated using H_2 at 1123 K for 0.5 h in a fixed-bed reactor, and the sample was pressed into a self-supporting 7-mm-diameter wafer under atmosphere, followed by treatment of the wafer with H_2 at 773 K for 0.5 h in a cell. After this pretreatment, the sample wafer was transferred to the measurement cell using a glove box filled with nitrogen, to avoid exposing the sample disk to air. The Rh K-edge EXAFS data were collected in a transmission mode at room temperature. The Co K-edge EXAFS data were collected in a fluorescence mode at room temperature. For the EXAFS analysis, oscillation was first extracted from EXAFS data using a spline smoothing method [25]. The oscillation was normalized by the edge height around 50 eV.

2.5. Titration of adsorbed oxygen during partial oxidation of methane

To examine the reduction degree of catalysts during partial oxidation of methane, titration of adsorbed oxygen with H_2 pulses was carried out after pulse reaction of partial oxidation of methane. The reactor was the same as that shown in Fig. 1b. Pulses of $CH_4 + O_2$ ($CH_4/O_2 = 2/1$) and H_2 were supplied using six-way valves. The pulse contents were 4.06 μmol CH_4 + 2.03 μmol O_2 and 0.045 μmol H_2. The amount of catalyst was 10 mg, with the amount of Rh as low as 0.31 μmol. The flow rate of the He carrier gas was 300 cm^3 min^{-1}. After H_2 pretreatment, the CH_4/O_2 pulse was introduced 10 times. Reactants and products were analyzed by quadrupole mass spectrometry (QMA200; Pfeiffer Vacuum Technology AG). Measurements of catalytic performance, such as CH_4 conversion, H_2 selectivity, and CO selectivity, were based on an average of 10 pulses.

2.6. Methane dissociation ability using a $CH_4 + D_2$ pulse

To evaluate methane dissociation activity, a pulse reaction of $CH_4 + D_2$ was carried out using the same apparatus as for the CH_4/O_2 reaction. Catalysts were reduced with hydrogen at 1123 K for 0.5 h before the CH_4–D_2 reaction. Pulse gases (CH_4/D_2 = 3.05/3.05 μmol) were introduced to the 10 mg of catalyst (Rh, 0.31 μmol) at flow rate of 30 cm^3 min^{-1} of the N_2 carrier.

3. Results and discussion

3.1. Catalytic performance in the partial oxidation of methane under isothermal conditions

Table 1 shows how the amount of Rh loading affects methane conversion and selectivity over Rh/MgO. The conversion and selectivity increased significantly with increasing Rh loading in the range of 0.3–1.0 wt% but remained almost constant in the range of 1.0–3.2 wt% Rh. This activity in the catalytic partial oxidation of methane was rather insensitive to the loading amount; this behavior agrees closely with that described previously [8]. It seems that the turnover frequency of the partial oxidation of methane decreased with increasing Rh loading.

Table 1 also summarizes the effects of adding a second metal over 0.3 wt% Rh/MgO. Adding Fe had a negative effect on the catalytic performance over Rh/MgO. This tendency can be related to the fact that Rh is the most effective component in catalytic partial oxidation of methane, as reported previously [7,8]. In contrast, adding Ni and Co promoted the partial oxidation of methane. Of particular interest is the finding that the performance of Rh–Co/MgO (Co/Rh = 1) with 0.3 wt% Rh exceeded that of 1.0 wt% Rh/MgO. At the same time, Rh–Co/MgO (Co/Rh = 1) gave a higher turnover frequency than the Rh/MgO catalysts. A promoting effect of Co addition also was observed on 0.6 wt% Rh–Co/MgO (Co/Rh = 1).

Table 2 summarizes the effects of adding Co over Rh–Co/MgO. Methane conversion and selectivity were improved by adding Co up to Co/Rh = 1; however, excessive Co, in the range of Co/Rh > 1, decreased the catalytic performance gradually. From the standpoint of conversion and TOF, the optimum amount of added Co was determined to be Co/Rh = 1 over 0.3 wt% Rh/MgO. H_2 adsorption increased with increasing amounts of Co on the Rh–Co/MgO catalysts. The maximum TOF was achieved at Co/Rh = 1. Table 2 also presents the results on 0.2 wt% Co/MgO. Based on the low catalytic

Table 1
Results of activity test in partial oxidation of methane with N_2 dilution and H_2 adsorption

Catalyst	H_2 adsorption ($\mu mol\ g_{cat}^{-1}$)[a]	Partial oxidation of methane			
		CH_4 conversion (%)[b]	H_2 selectivity (%)[b]	CO selectivity (%)[b]	TOF (s^{-1})[c]
0.3 wt% Rh/MgO	3.1	59	86	75	388
0.6 wt% Rh/MgO	5.5	67	86	77	248
1 wt% Rh/MgO	8.3	74	90	83	180
2 wt% Rh/MgO	15.9	78	92	88	99
3.2 wt% Rh/MgO	29.5	79	93	89	54
Rh–Co/MgO (Co/Rh = 1)	3.7	76	95	89	420
Rh–Ni/MgO (Ni/Rh = 1)	3.9	71	90	82	369
Rh–Fe/MgO (Fe/Rh = 1)	3.2	60	78	75	382
0.6 wt% Rh–Co/MgO (Co/Rh = 1)	6.3	83	95	90	268

[a] H_2 adsorption at 298 K.
[b] Reaction conditions: $CH_4/O_2/N_2 = 4/2/94$, total flow rate 1500 $cm^3\ min^{-1}$; $T_{TC} = 973$ K; total pressure 0.1 MPa; catalyst weight 10 mg; contact time 0.4 ms.
[c] Turnover frequency (TOF) in partial oxidation of methane is calculated on the basis of methane conversion rate and the amount of H_2 adsorption at 298 K.

Table 2
Results of activity test in partial oxidation of methane with N_2 dilution and H_2 adsorption

Catalyst	H_2 adsorption ($\mu mol\ g_{cat}^{-1}$)[a]	Partial oxidation of methane			
		CH_4 conversion (%)[b]	H_2 selectivity (%)[b]	CO selectivity (%)[b]	TOF (s^{-1})[c]
0.3 wt% Rh/MgO	3.1	59	86	75	388
Rh–Co/MgO (Co/Rh = 0.5)	3.3	63	90	78	391
Rh–Co/MgO (Co/Rh = 1)	3.7	76	95	89	420
Rh–Co/MgO (Co/Rh = 1.5)	3.7	71	88	83	391
Rh–Co/MgO (Co/Rh = 2)	4.1	59	79	72	291
Rh–Co/MgO (Co/Rh = 3)	4.1	54	75	71	266
0.2 wt% Co/MgO	–	1	2	30	–

[a] H_2 adsorption at 298 K.
[b] Reaction conditions: $CH_4/O_2/N_2 = 4/2/94$, total flow rate 1500 $cm^3\ min^{-1}$; $T_{TC} = 973$ K; total pressure 0.1 MPa; catalyst weight 10 mg; contact time 0.4 ms.
[c] Turnover frequency (TOF) in partial oxidation of methane is calculated on the basis of methane conversion rate and the amount of H_2 adsorption at 298 K.

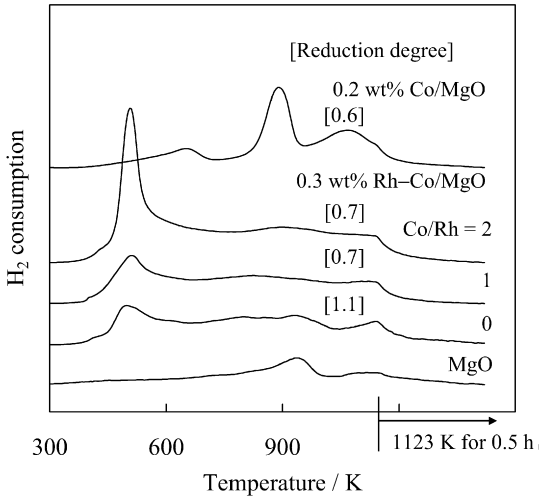

Fig. 2. TPR profiles of 0.3 wt% Rh–Co/MgO catalysts, as well as those of MgO and Co/MgO. Reduction degree was calculated as the following reactions: $Rh_2O_3 + 3H_2 \rightarrow 2Rh + 3H_2O$ and $Co_3O_4 + 4H_2 \rightarrow 3Co + 4H_2O$.

activity of the Co/MgO, an interaction between Rh and Co can be attributed to the better performance of the Rh–Co/MgO catalysts.

We also evaluated catalytic performance over the Rh–Co/MgO catalyst (Co/Rh = 1) after the reduction of H_2 at 1123 K for 3 h. The results were close to those seen after reduction for 0.5 h (Table 2), which can be related to the absence of H_2 consumption when the temperature was maintained at 1123 K for 0.5 h in the TPR profiles, as mentioned below.

3.2. Characterization of Rh–Co/MgO catalysts

Fig. 2 shows TPR profiles of the catalysts with H_2, and Table 3 presents H_2 consumption data. Reduction of Rh species on MgO proceeded in a wide temperature range. According to previous reports, H_2 consumption below 673 K was assigned to the reduction of Rh_2O_3, and H_2 consumption above 673 K was assigned to the reduction of $MgRh_2O_4$ [26–28]. The total amount of H_2 consumption on Rh/MgO was close to the stoichiometry of $Rh^{3+} + (3/2)H_2 \rightarrow Rh + 3H^+$, as presented in Table 3, indicating that almost all of the Rh species were present in a metallic state after the TPR experiment. On Co/MgO, the Co species on MgO were reduced at around 900 K [29]. For Rh–Co/MgO, a TPR peak at 500 K grew with increasing amounts of Co, where the H_2 was consumed by the reduction of Rh_2O_3 and Co_3O_4 species [30–32]. This behavior indicates that the Co species on Rh–Co/MgO were reduced along with the Rh_2O_3 species on MgO; the presence of Rh promoted the reduction of Co. In addition, the Rh and Co species interacting strongly with MgO, such as $MgRh_2O_4$, could be reduced at temperatures above 673 K. Based on the amount of H_2 consumption on Rh–Co/MgO (Co/Rh = 1 and 2) and considering H_2 consumption on Rh/MgO and MgO, about 70% of the Co species were reduced, given the assumption $Co_3O_4 + 4H_2 \rightarrow 3Co + 4H_2O$ (Table 3). The presence of unreduced Co species indicated a stronger interaction between Co and MgO compared with that between Rh and MgO.

Table 3
Results of temperature-programmed reduction and metal dispersion

Catalyst	Loading amount ($\mu mol\ g_{cat}^{-1}$)		H_2-TPR H_2 consumption ($\mu mol\ g_{cat}^{-1}$)	Amount of reduced Co[a] ($\mu mol\ g_{cat}^{-1}$)	Dispersion[b] (%)
	Rh	Co			
0.3 wt% Rh/MgO	31	0	52	–	10.1
Rh–Co/MgO (Co/Rh = 1)	31	31	63	23	6.9
Rh–Co/MgO (Co/Rh = 2)	31	62	107	45	5.3

[a] Assuming that all the Rh species are reduced ($Rh^{3+} \rightarrow Rh^0$) and stoichiometry of the Co reduction ($Co_3O_4 + 4H_2 \rightarrow 3Co + 4H_2O$).
[b] Dispersion was calculated as $(2 \times (H_2\ adsorption))/(Rh + reduced\ Co) \times 100$.

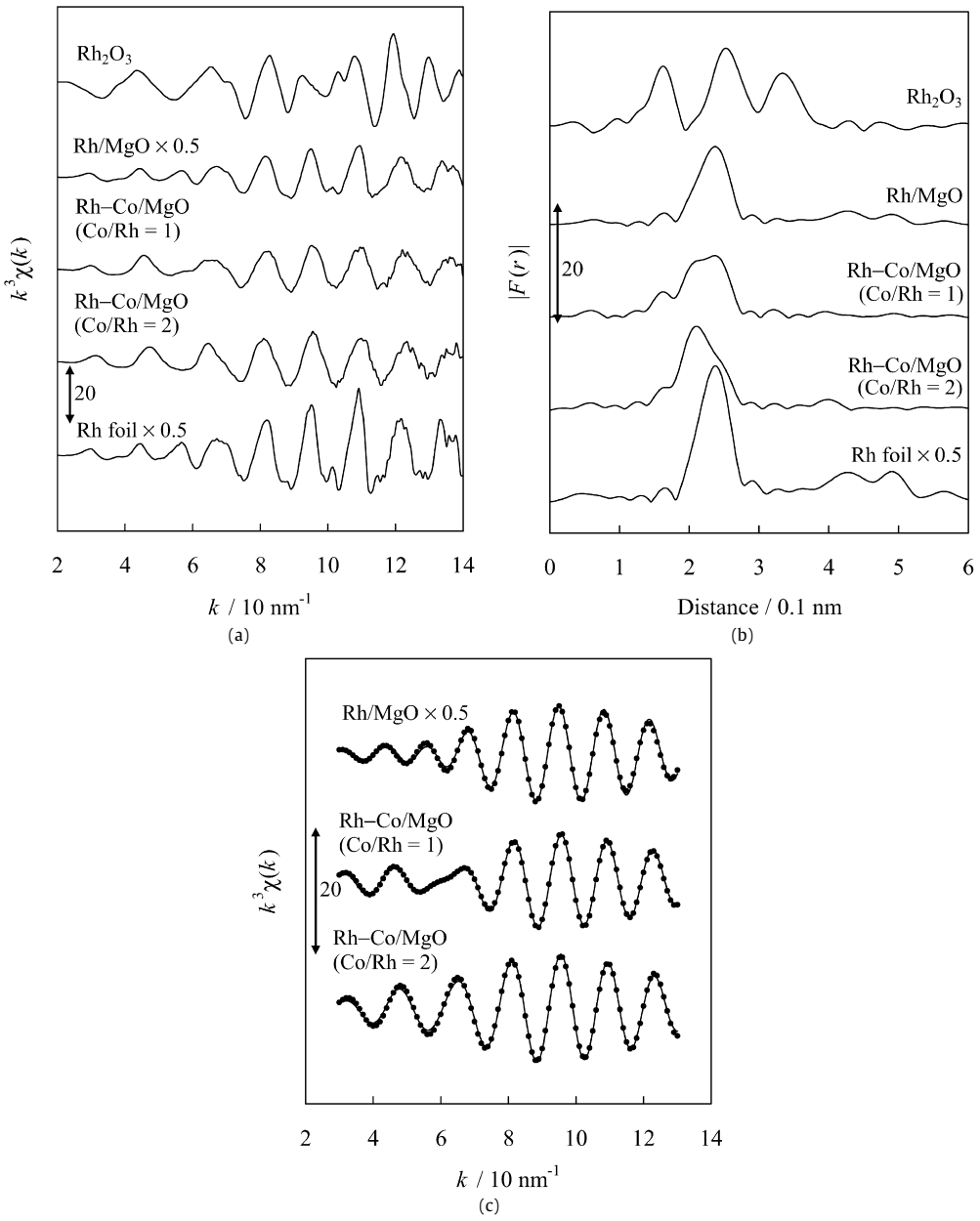

Fig. 3. Results of Rh K-edge EXAFS analysis of catalysts: (a) k^3-weighted EXAFS oscillations, (b) Fourier transform of k^3-weighted Rh K-edge EXAFS, FT range: 30–130 nm^{-1}, (c) Fourier filtered EXAFS data (solid line) and calculated data (dotted line).

EXAFS is very effective in analyzing the structural analysis of bimetallic catalysts when the information can be obtained from both edges of the components. Fourier transformation of the k^3-weighted EXAFS oscillation from k space to r space was performed to obtain a radial distribution function. Inversely Fourier-filtered data were analyzed using a curve-fitting method [33,34]. The Fourier transform and Fourier filtering ranges are shown for each result. For a curve-fitting analysis, the empirical phase shift and amplitude functions for the Rh–Rh, Rh–O, Co–Co, and Co–O bonds were extracted from data for Rh foil, Rh_2O_3, Co foil, and CoO. Theoretical functions for Rh–Co and Co–Rh bonds were calculated using the FEFF8.2 program [35]. Analyses of EXAFS data were performed using REX2000 version 2.3.3 software (Rigaku Corp). Error bars for each parameter in the curve-fitting procedure were estimated by stepping each parameter while optimizing the other parameters, until the R factor reached twice its minimum value [36]. Fig. 3 shows Rh K-edge EXAFS results of catalysts after H_2 reduction; Table 4 presents curve-fitting results. On the Rh–Co/MgO

Table 4
Curve fitting results of Rh K-edge EXAFS of reduced catalysts

Catalyst	Shell	CN[a]	R[b] (10^{-1} nm)	σ[c] (10^{-1} nm)	ΔE_0[d] (eV)	R_f[e] (%)
0.3 wt% Rh/MgO	Rh–Rh	10.6 ± 0.1	2.68 ± 0.01	0.076 ± 0.002	−0.2 ± 0.4	1.0
Rh–Co/MgO (Co/Rh = 1)	Rh–Rh	7.4 ± 0.2	2.64 ± 0.01	0.080 ± 0.004	−0.9 ± 0.4	0.5
	Rh–Co	3.2 ± 0.2	2.63 ± 0.02	0.080 ± 0.002	−2.2 ± 0.6	
Rh–Co/MgO (Co/Rh = 2)	Rh–Rh	5.7 ± 0.1	2.62 ± 0.01	0.078 ± 0.001	−1.7 ± 0.9	1.0
	Rh–Co	4.8 ± 0.1	2.57 ± 0.01	0.083 ± 0.005	−5.5 ± 0.7	
Rh foil	Rh–Rh	12.0	2.68	0.060	0	

[a] Coordination number.
[b] Bond distance.
[c] Debye–Waller factor.
[d] Difference in the origin of photoelectron energy between the reference and the sample.
[e] Residual factor. Fourier filtering range: 0.153–0.273 nm.

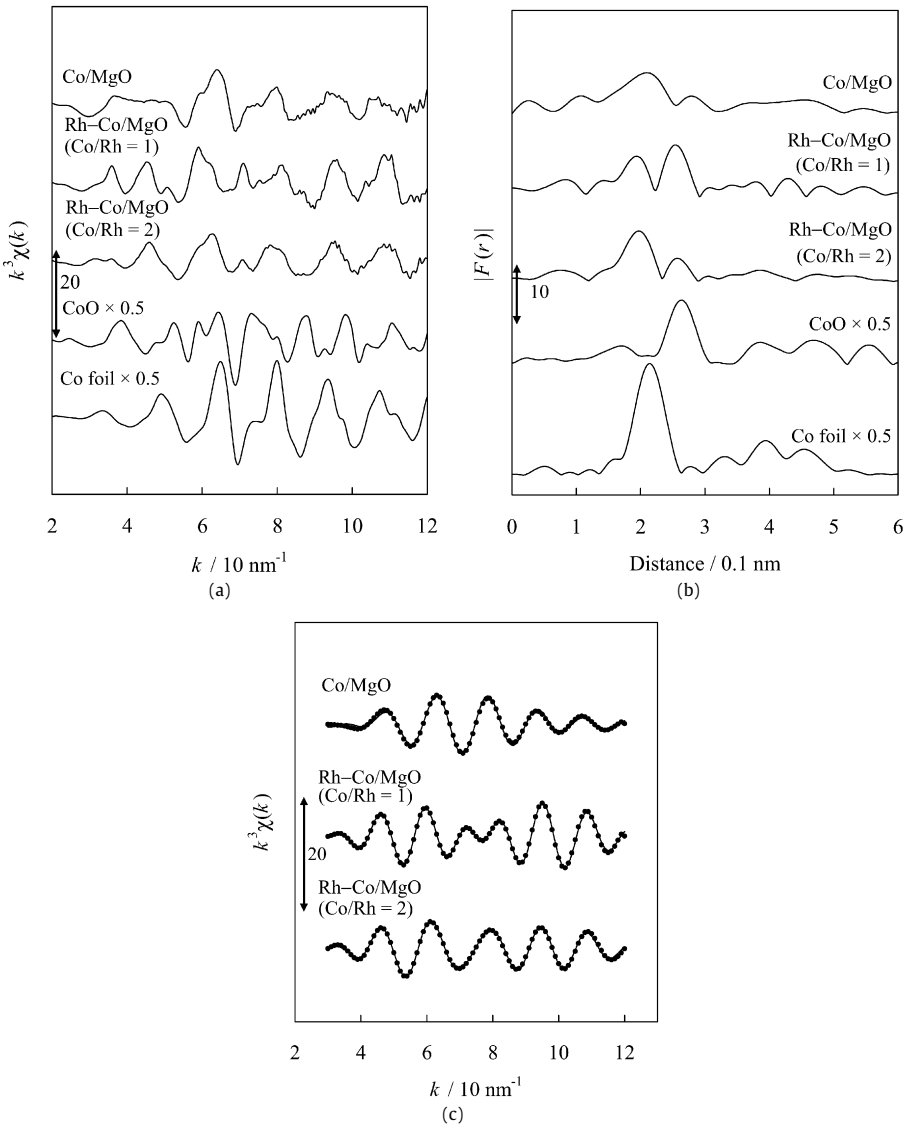

Fig. 4. Results of Co K-edge EXAFS analysis of catalysts: (a) k^3-weighted EXAFS oscillations, (b) Fourier transform of k^3-weighted Co K-edge EXAFS, FT range: 30–120 nm^{-1}, (c) Fourier filtered EXAFS data (solid line) and calculated data (dotted line).

catalysts, the Rh–Co bonds and Rh–Rh bonds were required to obtain good curve-fitting results. The coordination number (CN) of the Rh–Co bond increased and that of the Rh–Rh bond decreased with increasing amounts of Co. The bond distance of the Rh–Co bond was 0.257–0.263 nm, between the Rh–Rh bond (0.268 nm) in Rh metal and the Co–Co bond (0.251 nm) in Co metal. A similar bond length was reported previously [30]. At the same time, the Rh–Rh bond distance of 0.262–0.264 nm on the Rh–Co/MgO catalysts is shorter than that in Rh metal (0.268 nm). The curve-fitting results suggest alloy formation of Rh and Co [30–32,37–39].

Fig. 4 shows Co K-edge EXAFS results of catalysts after H_2 reduction. Table 5 presents curve-fitting results are presented in Table 5. For curve fitting of Co/MgO, both Co–Co and Co–O bonds are needed. In addition, the Co–Rh bond was also contributed on Rh–Co/MgO. The presence of the Co–O bond and its CN are supported by the Co-based reduction degree obtained from the TPR in the case of Rh–Co/MgO (Co/Rh = 1 and 2). As a result, EXAFS analysis and TPR results support the Rh–Co alloy formation. As reported previously, Ni was also alloyed with Rh easily [23]. On the other hand, it is expected that Fe is not alloyed with Rh easily, and this is why decreased performance was seen on Rh–Fe/MgO [40,41].

Table 5
Curve fitting results of Co K-edge EXAFS of reduced catalysts

Catalyst	Shell	CN[a]	R[b] (10^{-1} nm)	σ[c] (10^{-1} nm)	ΔE_0[d] (eV)	R_f[e] (%)
0.2 wt% Co/MgO	Co–Co	3.8 ± 0.1	2.50 ± 0.01	0.086 ± 0.016	−5.7 ± 2.1	0.7
	Co–O	2.9 ± 0.3	2.00 ± 0.03	0.093 ± 0.037	−6.6 ± 5.7	
Rh–Co/MgO (Co/Rh = 1)	Co–Co	3.3 ± 0.1	2.56 ± 0.01	0.084 ± 0.005	−9.5 ± 5.3	0.4
	Co–Rh	3.3 ± 0.1	2.62 ± 0.01	0.073 ± 0.010	10.0 ± 0.8	
	Co–O	2.4 ± 0.3	2.09 ± 0.01	0.070 ± 0.009	4.0 ± 0.2	
Rh–Co/MgO (Co/Rh = 2)	Co–Co	3.6 ± 0.2	2.54 ± 0.01	0.076 ± 0.005	−3.9 ± 0.5	0.6
	Co–Rh	2.4 ± 0.1	2.57 ± 0.01	0.081 ± 0.004	4.6 ± 0.6	
	Co–O	2.6 ± 0.3	2.13 ± 0.01	0.075 ± 0.015	8.3 ± 1.3	
CoO	Co–O	6.0	2.13	0.060	0	
Co foil	Co–Co	12.0	2.51	0.060	0	

[a] Coordination number.
[b] Bond distance.
[c] Debye–Waller factor.
[d] Difference in the origin of photoelectron energy between the reference and the sample.
[e] Residual factor. Fourier filtering range: 0.157–0.272 nm.

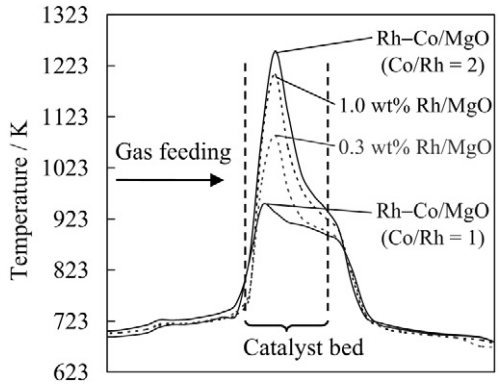

Fig. 5. Result of thermographical observation during partial oxidation of methane: (a) an example of a thermographical image on Rh–Co/MgO (Co/Rh = 1); (b) a picture of the catalyst bed; (c) temperature profiles of catalyst bed during the reaction from thermographical observation. Reaction conditions: $CH_4/O_2 = 2/1$; total flow rate 300 $cm^3\,min^{-1}$; total pressure 0.1 MPa; catalyst weight 10 mg; contact time 2.0 ms.

From the TEM observation, the average particle size of Rh/MgO and Rh–Co/MgO (Co/Rh = 1) after reduction is determined to be 5.5 ± 0.3 nm and 7.6 ± 0.3 nm, respectively. In the EXAFS analysis, the difference in particle size between Rh/MgO and Rh–Co/MgO (Co/Rh = 1) cannot be detected clearly because both sizes are too large to distinguish using EXAFS analysis. Increase of the particle size by Co addition can be associated with Rh–Co alloy formation because number of metallic atoms in a particle increases. In the reduction pretreatment, Rh species are reduced before the reduction of Co, and the reduced Co species are gradually incorporated into the Rh metal particles, which can explain the larger particle size of Rh–Co/MgO. The adsorption amount of H_2 and the metal dispersion on Rh/MgO and Rh–Co/MgO (Co/Rh = 1 and 2) are also presented in Table 1, where the stoichiometry of adsorbed hydrogen to surface metal Rh and Co atoms is assumed to be 1 [42,43]. Metal dispersion decreased with increasing amount of Co addition; this tendency agrees well with results obtained from TEM observations.

3.3. Catalytic performance in $CH_4/O_2 = 2/1$ without N_2 dilution

Regarding the partial oxidation of methane without dilution, the catalyst bed temperature is strongly influenced by the catalytic performance. Therefore, bed temperature profiles were measured using IR thermography. Fig. 5 shows the thermographical results over Rh–Co/MgO and Rh/MgO, at a fixed contact time. A very high temperature profile was detected near the bed inlet. The order of the highest bed temperature was as follows: Rh–Co/MgO (Co/Rh = 1) < 0.3 wt% Rh/MgO < 1.0 wt% Rh/MgO < Rh–Co/MgO (Co/Rh = 2). According to the previous report [8], H_2 and CO are formed in the presence of gas-phase oxygen by partial oxidation and in the absence of oxygen by steam reforming over the Rh catalyst. A similar interpretation is applicable to the profiles of 0.3 wt% and 1.0 wt% Rh/MgO. In addition, methane combustion as a side reaction in the presence of gas-phase oxygen also contributed to the temperature increase at the bed inlet. In contrast, the temperature profile on Rh–Co/MgO (Co/Rh = 1) was rather flat. This result indicates that addition of an optimum amount of Co is effective for suppression of hot spot formation over Rh/MgO.

Fig. 6 shows the effect of contact time on the highest bed temperature and catalytic performance in the partial oxidation of methane. Here, the contact time was increased by the decrease in flow rate at a constant catalyst amount. Conversion decreased with decreasing contact time, given a constant catalyst temperature. In the present case, CH_4 conversion increased with decreasing contact

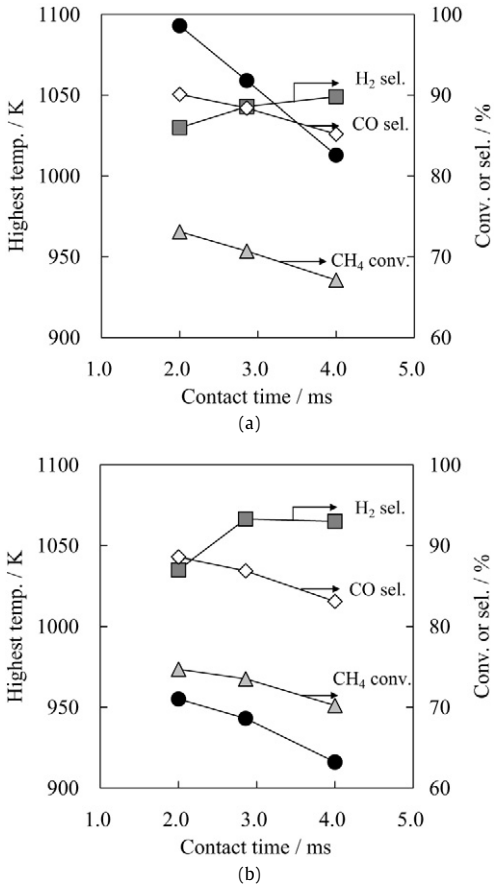

Fig. 6. Effect of contact time in partial oxidation of methane without N_2 dilution on the highest bed temperature and catalytic performance: (a) 0.3 wt% Rh/MgO, (b) Rh–Co/MgO (Co/Rh = 1). Reaction conditions: $CH_4/O_2 = 2/1$, total flow rate 300–150 $cm^3\,min^{-1}$; total pressure 0.1 MPa; catalyst weight 10 mg; contact time 2.0–4.0 ms.

Table 6
Comparison between the results of the activity tests and the equilibrium calculation

Catalyst or condition	Temperature (K)		CH_4 conv. (%)	H_2 sel. (%)	CO sel. (%)
	Highest bed	Outlet			
0.3 wt% Rh/MgO[a]	1093 ± 5	899 ± 5	73	86	90
Rh–Co/MgO[a] (Co/Rh = 1)	955 ± 5	885 ± 5	75	87	89
Equilibrium[b]		885	56	82	65
		899	62	84	70
		955	75	91	85

[a] Reaction Conditions: $CH_4/O_2 = 2/1$, total flow rate 300 $cm^3\,min^{-1}$; total pressure 0.1 MPa; catalyst weight 10 mg; contact time 2.0 ms.

[b] Equilibrium gas composition was calculated on the basis that the partial oxidation proceeds in an indirect route (the reforming reactions after the complete combustion of methane).

time, which indicates that the conversion is influenced by temperature increase more strongly than contact time decrease. On the other hand, Rh–Co/MgO (Co/Rh = 1) gave greater methane conversion than Rh/MgO at the same contact time and a lower bed temperature. Table 6 compares the results of the activity tests and the equilibrium gas composition calculated based on the assumptions that the reaction proceeds in an indirect reaction mechanism [18] and that methane-reforming reactions occur after methane combustion. In this case, methane conversion was limited by the reaction equilibrium of methane-reforming reactions with H_2O and CO_2, and the gas composition at the outlet temperature in the catalyst bed was determined on the basis of the equilibrium. The Rh–Co/MgO and Rh/MgO catalysts both exhibited greater conver-

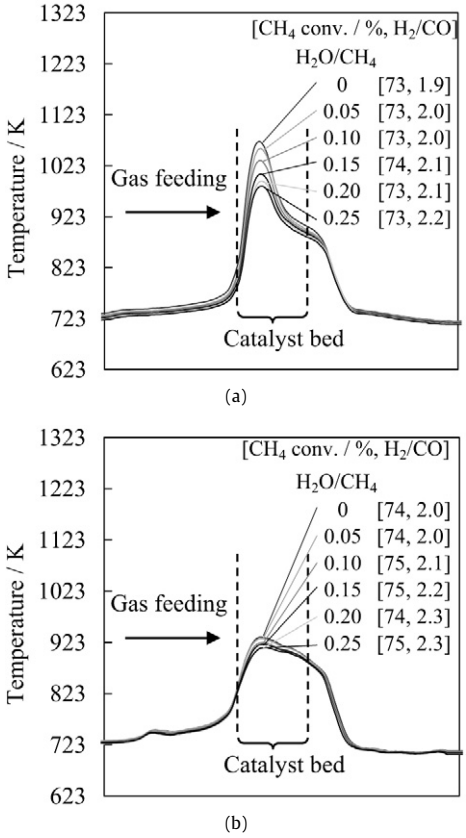

Fig. 7. Effect of steam addition to the partial oxidation of methane on temperature profiles: (a) 0.3 wt% Rh/MgO, (b) Rh–Co/MgO (Co/Rh = 1). Reaction conditions: $CH_4/O_2/H_2O$ = 200/100/0–50 $cm^3\,min^{-1}$, total flow rate 300–350 $cm^3\,min^{-1}$, H_2O/CH_4 = 0–0.25; total pressure 0.1 MPa; catalyst weight 10 mg; contact time 2.0–1.7 ms.

sion and selectivity than those at equilibrium based on the bed outlet temperature. In addition, the conversion and selectivity on Rh–Co/MgO were comparable to those at equilibrium based on the highest bed temperature seen. This behavior can be explained by the much smaller contribution of steam reforming on Rh–Co/MgO (Rh/Co = 1) than on 0.3 wt% Rh/MgO. This behavior was seen more clearly in the partial oxidation of methane in the presence of steam, as described below. In addition, Rh–Co/MgO characteristically yielded greater methane conversion when the highest bed and outlet temperatures were lower than those for Rh/MgO. Conversion and selectivity are favored at higher temperatures [44], and hot spot formation can promote the partial oxidation of methane through heat transfer over Ni/Yb_2O_3. This can be attributed to the steam reforming of methane promoted by the heat from the combustion reaction. The opposite tendency was seen in the present study, which can be attributed to the much smaller contributions of steam reforming and the much greater contribution of direct partial oxidation, as discussed below.

Fig. 7 shows the effect of steam addition on the temperature profiles of the catalyst bed. For Rh/MgO, the highest bed temperature decreased significantly with increasing partial pressure of steam. This behavior can result from an increasing contribution of steam reforming of methane, a highly endothermic process. Based on previous reports [45,46], the kinetics of steam reforming of methane are independent of steam partial pressure. Therefore, we conclude that the addition of steam increased the amount of the active metallic species by increasing the H_2 partial pressure, because the Rh species were partially oxidized at the inlet of the catalyst bed. In contrast, the partial pressure of steam had no significant affect on the temperature profiles on Rh–Co/MgO (Co/Rh = 1). This tendency also was supported by the lower catalytic activity in steam reforming over Rh–Co/MgO (Co/Rh = 1) than over Rh/MgO (data not shown). Flat temperature profiles on Rh–Co/MgO (Co/Rh = 1) can be affected by two factors: greater selectivity for the direct catalytic partial oxidation of methane (a less exothermic reaction) and a reduction in the steam-reforming reaction (a highly endothermic reaction). Both of these factors can contribute to the suppression of hot spot formation through the addition of Co.

Table 7
Catalytic performance of pulse $CH_4 + O_2$ reaction and reduction degree after the reaction

Catalyst	Pulse $CH_4 + O_2$ reaction[a]			Reduction degree (%)[b]
	CH_4 conversion (%)	H_2 selectivity (%)	CO selectivity (%)	
0.3 wt% Rh/MgO	56	62	55	59
Rh–Co/MgO (Co/Rh = 1)	66	78	75	89
Rh–Co/MgO (Co/Rh = 2)	5	9	13	33

[a] Reaction conditions: CH_4/O_2 = 4.06/2.03 μmol (300 $cm^3\,min^{-1}$ He carrier); T_{TC} = 873 K; total pressure 0.1 MPa; catalyst weight 10 mg (0.31 μmol_{Rh}).
[b] Reduction degree was based on H_2 consumption in titration of adsorbed oxygen with H_2 pulses and calculated as (the H_2 consumption after the pulse $CH_4 + O_2$ reaction)/(the H_2 consumption after O_2 oxidation treatment at 873 K) ×100.

3.4. Reduction degree during the reaction and methane dissociation ability

Table 7 summarizes the results of the CH_4/O_2 pulse reaction and subsequent titration of adsorbed oxygen species. In the CH_4/O_2 pulse reaction, the amount of CH_4 and O_2 feed greatly exceeded the number of surface metal atoms. The order of methane conversion in the pulse experiment was the same as that in activity tests under continuous-flow conditions. Consequently, we believe that the steady-state catalyst surface was reproduced in the pulse experiment. We measured the amount of adsorbed and absorbed oxygen by the reaction of H_2 ($O(a) + H_2 \rightarrow H_2O$) after the pulse reaction; the total amount of H_2 consumed in the pulses gave the reduction degree of Rh and Co. The degree of reduction was calculated based on the amount of H_2 consumption on catalysts oxidized under 100% O_2 at 873 K for 30 min. The degree of reduction was rather small and cannot be explained by the amount of adsorbed oxygen on the metal surface. In particular, the bulk metallic species also were oxidized during the reaction on Rh/MgO and Rh–Co/MgO (Co/Rh = 2). A clear relationship was seen between the performance in the partial oxidation of methane and the degree of reduction. The catalysts with lower degree of reduction had lower conversion and selectivity. This tendency indicates that methane can be activated on the metal surface and not on the oxidized surface [47,48]. An interesting finding is the order of the reduction degree during the reaction: Rh–Co/MgO (Co/Rh = 1) > Rh/MgO > Rh–Co/MgO (Co/Rh = 2). As may be apparent, Co had a much greater oxygen affinity than Rh [49]; greater oxygen affinity should result in greater amounts of adsorbed and absorbed oxygen during the reaction and a lower degree of reduction. This expectation was found to hold true for Rh–Co/MgO (Co/Rh = 2) but not for Rh–Co/MgO (Co/Rh = 1). The state of Rh and Co species during the CH_4/O_2 pulse reaction depended on the reduction rate of the oxidized species and the oxidation rate of the reduced species. The rate of oxidation can increase with Co content because of its high oxygen affinity. On the other hand, in terms of the reduction rate, when the reducibility agent is H_2, the rate of reduction of the Rh/MgO and Rh–Co/MgO catalysts would be expected to be almost the same as that shown in the TPR profiles (Fig. 2). But in fact, the reducing agents for the reaction can be methane, H_2, and CO, and the pressure of the reducing agents also can depend on the catalytic activity. The Rh and Co species tended to be present as

Table 8
CH_4–D_2 exchange reaction over 0.3 wt% Rh/MgO and Rh–Co/MgO (Co/Rh = 1.0 and 2.0)

Catalyst	Composition (%)[a]				
	CH_4	CH_3D	CH_2D_2	CHD_3	CD_4
0.3 wt% Rh/MgO	94	0.5	0.6	1.6	3.6
Rh–Co/MgO (Co/Rh = 1)	92	0.4	1.0	2.4	4.3
Rh–Co/MgO (Co/Rh = 2)	97	0.3	0.3	0.5	2.1

[a] Reaction conditions: CH_4/D_2 = 3.05/3.05 μmol (30 $cm^3\,min^{-1}$ N_2 carrier); T_{TC} = 573 K; total pressure 0.1 MPa; catalyst weight 10 mg (0.31 μmol_{Rh}).

metallic species when an optimum amount of Co was added, because high catalytic activity could compensate for the increase of the oxidation rate. In contrast, when too much Co was added, the oxidation rate exceeded the reduction rate significantly.

Table 8 gives the CH_4–D_2 reaction results at 573 K for the evaluation of methane dissociation ability. This ability was ordered as follows: Rh–Co/MgO (Co/Rh = 1) > Rh/MgO > Rh–Co/MgO (Co/Rh = 2). Rh–Co/MgO (Co/Rh = 2) demonstrated a rather low ability despite the high H_2 adsorption. Previous studies on the steam reforming of methane have shown that the Co metal surface has less methane activation ability than the Rh metal surface [50]. This property may be connected to the poor performance in the dissociation and partial oxidation of methane. In contrast, Rh–Co/MgO (Co/Rh = 1) has better methane dissociation ability than Rh/MgO, due in part to greater H_2 adsorption on Rh–Co/MgO (Co/Rh = 1) (Table 3). Based on the EXAFS results, we suggest that the surface Co atoms on the Rh–Co alloy particles with a suitable composition can contribute to the dissociation and partial oxidation of methane, the performance of which is comparable to that of Rh atoms on Rh–Co alloy and Rh metal particles. At present, the promotion mechanism of methane dissociation on Rh–Co/MgO (Co/Rh = 1) remains unclear; further investigation is needed.

4. Conclusion

For the partial oxidation of methane with N_2 dilution, Rh–Co/MgO (Co/Rh = 1) exhibited higher activity and selectivity to H_2 and CO compared with 0.3 wt% and 1.0 wt% Rh/MgO. Characterization by TPR and EXAFS indicated the formation of a Rh–Co alloy on the Rh–Co/MgO catalysts; this also was supported by TEM and adsorption measurements.

In the partial oxidation of methane without N_2 dilution, Rh–Co/MgO (Co/Rh = 1) had much lower catalyst bed temperatures than Rh/MgO. The addition of steam significantly decreased the highest bed temperature on Rh/MgO. In contrast, the temperature profile was not affected by the addition of steam on Rh–Co/MgO (Co/Rh = 1). These results indicate that Rh/MgO catalyzed the partial oxidation and combustion of methane at the bed inlet in the presence of gas-phase oxygen, which increased the temperature dramatically. Downstream, the steam reforming of methane was catalyzed in the absence of oxygen. The addition of Co promoted the partial oxidation of methane and suppressed the combustion of methane over Rh–Co/MgO (Co/Rh = 1) in the presence of gas-phase oxygen, resulting in the suppression of hot spot formation. The flat bed temperature profiles on Rh–Co/MgO (Co/Rh = 1) could be simultaneously affected by two factors: greater selectivity for the direct partial oxidation of methane and reduced steam reforming of methane. Titration of adsorbed oxygen during the reaction revealed that a greater reduction degree on Rh–Co/MgO (Co/Rh = 1) than on Rh/MgO, which is associated with greater methane dissociation ability. The results can explain the good performance of Rh–Co/MgO (Co/Rh = 1), and the catalytic performance of Rh–Co/MgO may depend on the surface composition of the Rh–Co alloy particles.

Acknowledgments

Financial support was provided by the Japan Oil, Gas and Metals National Corporation and Chiyoda Corporation.

References

[1] J.R. Rostrup-Nielsen, J. Sehested, J.K. Nørskov, Adv. Catal. 47 (2002) 65.
[2] J.R. Rostrup-Nielsen, in: J.R. Anderson, M. Boudart (Eds.), Catalysis Science and Technology, Springer-Verlag, Berlin, 1984, p. 1.
[3] K. Aasberg-Petersen, J.-H. Bak Hansen, T.S. Christensen, I. Dybkjaer, P.S. Christensen, C. Stub Nielsen, S.E.L. Winter Madsen, J.R. Rostrup-Nielsen, Appl. Catal. A 221 (2001) 379.
[4] J.R. Rostrup-Nielsen, Catal. Rev. 46 (2004) 247.
[5] A.P.E. York, T. Xian, M.L.H. Green, J.B. Claridge, Catal. Rev. 49 (2007) 511.
[6] D.A. Hickman, L.D. Schmidt, J. Catal. 138 (1992) 267.
[7] D.A. Hickman, L.D. Schmidt, Science 259 (1993) 343.
[8] R. Horn, K.A. Williams, N.J. Degenstein, A. Bitsch-Larsen, D. Dalle Nogare, S.A. Tupy, L.D. Schmidt, J. Catal. 249 (2007) 380.
[9] R. Horn, N.J. Degenstein, K.A. Williams, L.D. Schmidt, Catal. Lett. 110 (2006) 169.
[10] K.L. Hohn, L.D. Schmidt, Appl. Catal. A 211 (2001) 53.
[11] R. Horn, K.A. Williams, N.J. Degenstein, L.D. Schmidt, J. Catal. 242 (2006) 92.
[12] R. Horn, K.A. Williams, N.J. Degenstein, L.D. Schmidt, Chem. Eng. Sci. 62 (2007) 1298.
[13] C. Elmasides, T. Ioannides, X.E. Verykios, AIChE J. 46 (2000) 1260.
[14] B.C. Enger, R. Lødeng, A. Holmen, Appl. Catal. A 346 (2008) 1.
[15] B. Li, S. Kado, Y. Mukainakano, T. Miyazawa, T. Miyao, S. Naito, K. Okumura, K. Kunimori, K. Tomishige, J. Catal. 245 (2007) 144.
[16] Y. Mukainakano, B. Li, S. Kado, T. Miyazawa, K. Okumura, T. Miyao, S. Naito, K. Kunimori, K. Tomishige, Appl. Catal. A 318 (2007) 252.
[17] A.M.D. Groote, G.F. Froment, Appl. Catal. A 138 (1996) 245.
[18] D. Dissanayake, M.P. Rosynek, K.C.C. Kharas, J.H. Lunsford, J. Catal. 132 (1991) 117.
[19] I. Tavazzi, A. Beretta, G. Groppi, P. Forzatti, J. Catal. 241 (2006) 1.
[20] L. Basini, K. Aasber-Petersen, A. Guarinoni, M. Ostberg, Catal. Today 64 (2001) 9.
[21] B. Li, K. Maruyama, M. Nurunnabi, K. Kunimori, K. Tomishige, Ind. Eng. Chem. Res. 44 (2005) 485.
[22] B. Li, R. Watanabe, K. Maruyama, M. Nurunnabi, K. Kunimori, K. Tomishige, Appl. Catal. A 290 (2005) 36.
[23] B. Li, K. Maruyama, M. Nurunnabi, K. Kunimori, K. Tomishige, Appl. Catal. A 275 (2004) 157.
[24] Y. Chen, K. Tomishige, K. Yokoyama, K. Fujimoto, Appl. Catal. A 165 (1997) 335.
[25] J.W. Cook, D.E. Sayers, J. Appl. Phys. 52 (1981) 5024.
[26] H.Y. Wang, E. Ruckenstein, J. Catal. 186 (1999) 181.
[27] E. Ruckenstein, H.Y. Wang, J. Catal. 190 (2000) 32.
[28] E. Ruckenstein, H.Y. Wang, Appl. Catal. A 198 (2000) 33.
[29] E. Ruckenstein, H.Y. Wang, Appl. Catal. A 204 (2000) 257.
[30] H.F.J. Van't Blik, D.C. Koningsberger, R. Prins, J. Catal. 97 (1986) 210.
[31] H.F.J. Van't Blik, R. Prins, J. Catal. 97 (1986) 188.
[32] J.H.A. Martens, H.F.J. Van't Blik, R. Prins, J. Catal. 97 (1986) 200.
[33] K. Okumura, J. Amano, N. Yasunobu, M. Niwa, J. Phys. Chem. B 104 (2000) 1050.
[34] K. Okumura, S. Matsumoto, N. Nishiaki, M. Niwa, Appl. Catal. B 40 (2003) 151.
[35] A.L. Ankudinov, B. Ravel, J.J. Rehr, S.D. Conradson, Phys. Rev. B 58 (1998) 7565.
[36] K. Tomishige, K. Asakura, Y. Iwasawa, J. Catal. 149 (1994) 70.
[37] H. Kusama, K. Okabe, H. Arakawa, Appl. Catal. A 207 (2001) 85.
[38] M. Ichikawa, J. Catal. 56 (1979) 127.
[39] M. Ichikawa, J. Catal. 59 (1979) 67.
[40] J.W. Niemantsverdriet, A.M. Van der Kraan, W.N. Delgass, J. Catal. 89 (1984) 138.
[41] A. Fukuoka, T. Kimura, N. Kosugi, H. Kuroda, Y. Minai, Y. Sakai, T. Tominaga, M. Ichikawa, J. Catal. 126 (1990) 434.
[42] K. Kunimori, T. Uchijima, M. Yamada, H. Matsumoto, T. Hattori, Y. Murakami, Appl. Catal. 4 (1982) 67.
[43] R.C. Reuel, C.H. Bartholomew, J. Catal. 85 (1984) 63.
[44] D. Dissanayake, M.P. Rosynek, J.H. Lunsford, J. Phys. Chem. 97 (1993) 3644.
[45] J. Wei, E. Iglesia, J. Catal. 225 (2004) 116.
[46] J. Wei, E. Iglesia, Angew. Chem. Int. Ed. 43 (2004) 3685.
[47] T. Sasaki, K. Nakao, K. Tomishige, K. Kunimori, Appl. Catal. A 328 (2007) 140.
[48] T. Sasaki, K. Nakao, K. Tomishige, K. Kunimori, Chem. Commun. (2006) 3821.
[49] T.B. Reed, Free Energy Formation of Binary Compounds, MIT Press, Cambridge, MA, 1971, p. 67.
[50] E. Kikuchi, S. Tanaka, Y. Yamazaki, Y. Morita, Bull. Jpn. Petrol. Inst. 16 (1974) 95.